

THE SIMULATION OF BIOGAS COMBUSTION IN A MILD BURNER

M. M. Noor^{1,3}, Andrew P. Wandel¹ and Talal Yusaf²

¹Computational Engineering and Science Research Centre, School of Mechanical and Electrical Engineering, University of Southern Queensland (USQ), Australia

²National Center for Engineering in Agriculture, USQ, Australia

³Faculty of Mechanical Engineering, University of Malaysia Pahang, Malaysia
Email: muhamad@ump.edu.my

ABSTRACT

This paper discusses the design and development of moderate and intense low oxygen dilution (MILD) combustion burners, including details of the computational fluid dynamics process, step-by-step from designing the model until post-processing. A 40 mm diameter bluff-body burner was used as the flame stabilizer. The fuel nozzle was placed in the center with a diameter of 1mm and an annular air nozzle with an opening size of 1,570 mm², and four EGR pipes were used. Non-premixed combustion with a turbulent realizable *k*-epsilon was used in the simulation. The fuel used is low calorific value gas (biogas). The synthetic biogas was a mixture of 60% methane and 40% carbon dioxide. The simulation was successfully achieved during the MILD regime where the ratio of maximum-to-average temperature was less than the required 23%.

Keywords: Combustion; computational fluid dynamics; bluff-body; low calorific value gas; MILD burner; biogas.

INTRODUCTION

Combustion is still the most important process in generating energy. The improvement of combustion efficiency will have a major impact on the cost of energy. The high and growing demand for energy in today's world has been met to approximately 80% by the fossil fuel supply (IEA, 2009; Maczulak, 2010). Fossil fuel reserves are questionable (Shafiee & Topal, 2009) and the use of fossil fuel has resulted in an increase in the emission of unwanted pollutants (Khelil, Naji, & Loukarfi, 2007; Yusaf, Noor, & Wandel, 2013). This condition requires urgent development of an improved pollutants process and new sources of energy other than fossil fuels. Biogas is one of the options since it is renewable, and carbon dioxide produced in the combustion process will be used in return by the biomass that is grown to produce biogas. Moderate and intense low oxygen dilution (MILD) combustion is proven to improve thermal efficiency and reduce NO_x emissions (Cavaliere & Joannon, 2004; Dally, Shim, Craig, Ashman, & Szegö, 2010; Li et al., 2011; Noor, Wandel, & Yusaf, 2012; Noor, M. M., Wandel, A. P., & Yusaf, T., 2013a). This combustion technique is also called flameless oxidation, or FLOX (Wünning, 1991), high temperature air combustion (Katsuki & Hasegawa, 1998; Tsuji et al., 2003) or colorless distributed combustion (Arghode & Gupta, 2011). Real model development and fabrication, and repeating the process until the desired result, is costly at the design stage of any engineering equipment. Computational fluid dynamics (CFD) is one of the ways to virtually design and run a simulation experiment without the need to physically build a model. This process can be carried out using

commercial software and is much cheaper compared to physical model building. CFD has been successful in carrying out simulations of many engineering problems (Baukal Jr, Gershtein, & Li, 2000; Davidson, 2002), such as those for gas turbines (Duwig, Stankovic, Fuchs, Li, & Gutmark, 2007), industrial furnaces (Chen, Yong, & Ghoniem, 2012), boilers (Rahimi, Khoshhal, & Shariati, 2006), internal combustion engines (Devi, Saxena, Walter, Record, & Rajendran, 2004), MILD or flameless combustors (Acon, Sala, & Blanco, 2007; Hasegawa, Mochida, & Gupta, 2002; Noor, M. M., Wandel, A. P., & Yusaf, T., 2013b; Verissimo, Rocha, & Costa, 2013) and other engineering applications (Fletcher, Haynes, Christo, & Joseph, 2000; Najiha, Rahman, Kamal, Yusoff, & Kadirgama, 2012; Ramasamy et al., 2009; Wandel, Smith, & Klimenko, 2003). Simulations can also be run using discretization of fluid flow equations through the finite difference method (FDM) and Taylor expansion, then writing the coding using FORTRAN (Noor, Hairuddin, Wandel, & Yusaf, 2012; Press, Teukolsky, Vetterling, & Flannery, 1992) or MATLAB (Hairuddin, Yusaf, & Wandel, 2011; Wandel, 2011, 2012). The purpose of this study is to design and develop a model for the MILD combustion burner. This paper drafts, step by step, a CFD simulation for the non-premixed MILD combustion furnace with biogas as a fuel. In addition to experimental testing, computational work is now becoming more and more important due to its lower cost and acceptable accuracy with minimum error. Especially in newly developed models, computational testing using CFD software will reduce much trial and error in experimental work.

CFD GOVERNING EQUATIONS

The governing equations for the CFD calculations are the fluid flow and turbulence governing equations. The equations involve a series of fluid properties; mass conservation (continuity equation), density, temperature, species, mass fraction, enthalpy, turbulent kinetic energy (k) and turbulent dissipation rate (ϵ). For the axisymmetric flow in low Mach number ($M < 0.3$) (Majda & Sethian, 1985; Rehm & Baum, 1978), the transport equations are:

Mass (the continuity equation)

$$\frac{\partial \rho}{\partial t} + \nabla \cdot \rho U = 0 \quad (1)$$

Momentum

$$\frac{\partial \rho U}{\partial t} + (\nabla \cdot \rho U U) = -\nabla p + \nabla \cdot \tau + \rho g \quad (2)$$

Enthalpy

$$\frac{\partial \rho h}{\partial t} + \nabla \cdot \rho U = \nabla \cdot \lambda_e \nabla T - \nabla \cdot q_{rad} + \nabla \cdot \sum_l \rho h_l(T) D_e \nabla m_l \quad (3)$$

Temperature

$$\rho c_p \frac{DT}{Dt} = \nabla \cdot \lambda_e \nabla T - \nabla \cdot \sum_l \rho h_l(T) D_e \nabla m_l - \rho \sum_l \frac{Dm_l}{Dt} h_l(T) \quad (4)$$

Species mass fraction

$$\frac{\partial \rho m_l}{\partial t} + \nabla \cdot \rho U m_l = \nabla \cdot D_e \rho \nabla m_l - R_l \quad (5)$$

The most common turbulent model is the k- ϵ model (Jones and Launder, 1972; Launder and Sharma, 1974). This model was practical for many flows, and relatively

simple to implement and easy to converge. The equation for turbulent kinetic energy (k) is Equation (6) and turbulent dissipation rate (ϵ) is Equation (7).

$$\frac{\partial}{\partial t}(\rho k) + \frac{\partial}{\partial x_i}(\rho k u_i) = \frac{\partial}{\partial x_j} \left[\left(\mu + \frac{\mu_t}{\sigma_k} \right) \frac{\partial k}{\partial x_j} \right] + P_k + P_b - \rho \epsilon - Y_M + S_k \quad (6)$$

$$\frac{\partial}{\partial t}(\rho \epsilon) + \frac{\partial}{\partial x_i}(\rho \epsilon u_i) = \frac{\partial}{\partial x_j} \left[\left(\mu + \frac{\mu_t}{\sigma_\epsilon} \right) \frac{\partial \epsilon}{\partial x_j} \right] + C_{1\epsilon} \frac{\epsilon}{k} (P_k + C_{3\epsilon} P_b) - \rho C_{2\epsilon} \frac{\epsilon^2}{k} + S_\epsilon \quad (7)$$

where turbulent viscosity, $\mu_t = \rho C_\mu \frac{k^2}{\epsilon}$, production of k , $P_k = -\overline{\rho u'_i u'_j} \frac{\partial u_j}{\partial x_i}$, and effect of buoyancy, $P_b = \beta g_i \frac{\mu_t}{Pr_t} \frac{\partial T}{\partial x_i}$ and $\beta = -\frac{1}{\rho} \left(\frac{\partial \rho}{\partial T} \right)_p$. In the effect of buoyancy, g_i is the component of the gravitational vector in the i th direction and Pr is turbulent Prandtl number. Pr is 0.85 for the standard and realizable k - ϵ model. Other model constants are $C_{1\epsilon}$, $C_{2\epsilon}$, $C_{3\epsilon}$, C_μ , σ_k and σ_ϵ . The common fluid flow problems can be solved in one, two or three dimensions with parabolic, elliptic or hyperbolic equations.

MODEL DEVELOPMENT

The modeling simulation was designed and developed using ANSYS design modeler software as in Figure 1. In order to expedite the solution, the model must be small and simple, but meet the required model drawing and shape, because the smaller the model, the fewer meshing nodes and elements to be calculated later. The mesh grid quantity will directly impact the solution duration. If the model is symmetrical, it can be halved (Figure1(b)) or even quartered (Figure1(c)). The geometry of the model includes volumes, surface, edges and vertices. All of these items can be taken into account in meshing techniques.

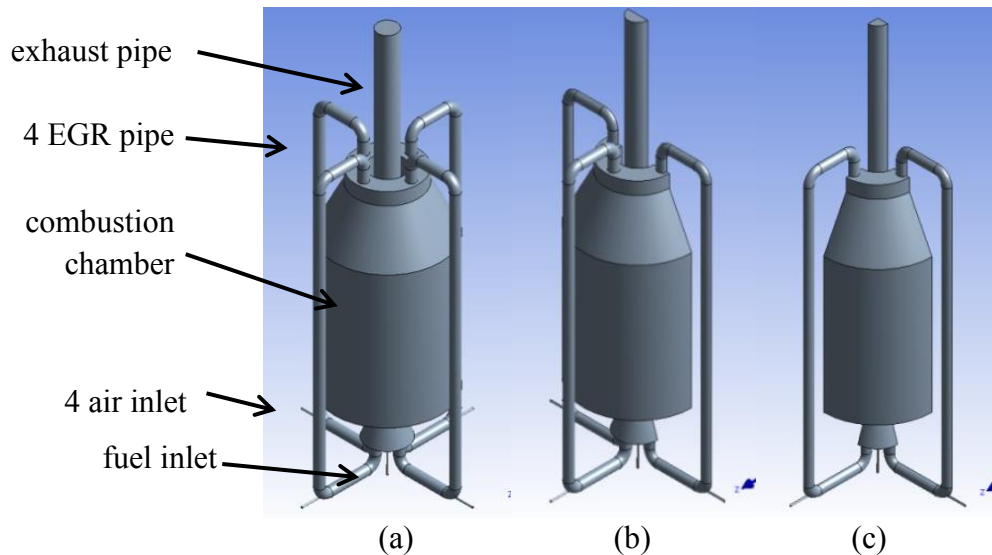


Figure 1: MILD furnace (a) the model schematic diagram with boundary condition, (b) half model axisymmetric at xy -plane, (c) quarter model axisymmetric at xy -plane and yz -plane

MODEL MESHING

The model meshing is the most important and sensitive process in CFD simulations. The quality of meshing will be determined by the technique of the meshing. Meshing will create a grid of cells or elements which are required to solve all the desired fluid flow equations. The size of the grid will give significant impact on the computational time which has direct impact on the cost of simulations. The grid will also have a significant effect on the convergence speed and solution accuracy. Industrial CFD problems normally consist of large numerical grid cells (Peters, 2004). In the meshing process, inflation must be applied for the area near the wall or near the boundary layer mesh. Figures 2(a) and 2(b) show the plain meshing without inflation and detail sizing of some important areas. Figures 2(c) and 2(d) show the meshing with inflation and the nozzle area with the body of influence and edge sizing technique. The meshing process is highly complex and much practice, trial and error is required for its skilled use. Practice can be gained following the ANSYS meshing tutorial available on their website. The meshing process must be start with coarse mesh (Table 1), using statistics to check the quality (Table 2). The required quality check is of the skewness and aspect ratio on mesh metrics and smoothness (changes in cell size). The maximum skewness must be below 0.98 or the solution will easily become a divergence error and will not converge as desired (Noor, M., Wandel, A. P., & Yusaf, T., 2013). Some models and settings may have different limit ranges, from 0.85 to 0.98. The overall range of skewness is from zero to one, where the best is zero and worst is one. The skewness value is calculated based on equilateral or equiangular shape. For example the skewness for equilateral is the ratio of the optimal cell size minus the actual cell size divided by the optimal cell. In this case, coarse mesh gives a maximum skewness of 0.9817, which is higher than the allowable value. A medium or fine mesh is needed to ensure the skewness is below 0.98. When the meshing uses a fine relevance center and other setting as final setting in Table 1, the maximum skewness is lowered to 0.8458, and is below the most rigid limit of 0.85.

Table 1. Mesh sizing setting parameters

Sizing Parameters	Beginning Setting	Final Setting
Advance size function	Proximity and curvature	Proximity and curvature
Relevance center	Coarse	Fine
Initial size seed	Active assembly	Active assembly
Smoothing	Low	High
Transition	Fast	Slow
Span angle center	Coarse	Fine
Curvature normal angle	Default (70.3950°)	Default (18.0°)
Proximity min size	0.5	0.5
Num cells across gap	Default (3)	Default (3)
Min size	Default (1.21770mm)	Default (0.356650mm)
Proximity min size	Default (1.21770mm)	Default (0.356650mm)
Max face size	Default (121.770mm)	Default (35.6650mm)
Max size	Default (243.540mm)	Default (71.3290mm)
Growth rate	Default (1.850)	Default (1.20)
Minimum	1.0mm	1.2mm

The aspect ratio is calculated by dividing the longest edge length by the shortest edge. An aspect ratio of 1.0 is the best and means that the cell is nicely square or has equal edge lengths of any shape. The cell shapes were triangular and quadrilateral for the 2D problem and tetrahedron, hexahedron, pyramid wedges and polyhedrons for the 3D problem. The smoothness or the change in cell size must be gradual and must not be more than 20% change from one cell to the next. If there are cells that jump in size, the smoothness will be very bad and the solution will be hard to converge. The node and element quantity is critical since it will affect the final result and the computational time, which involves computational cost. A higher meshing element will give a better final result, but takes longer computational time to complete the simulation. At this point, the acceptable mesh quality will be the best solution for both an acceptable final result and computational time. The dynamic mesh is not applicable to this problem.

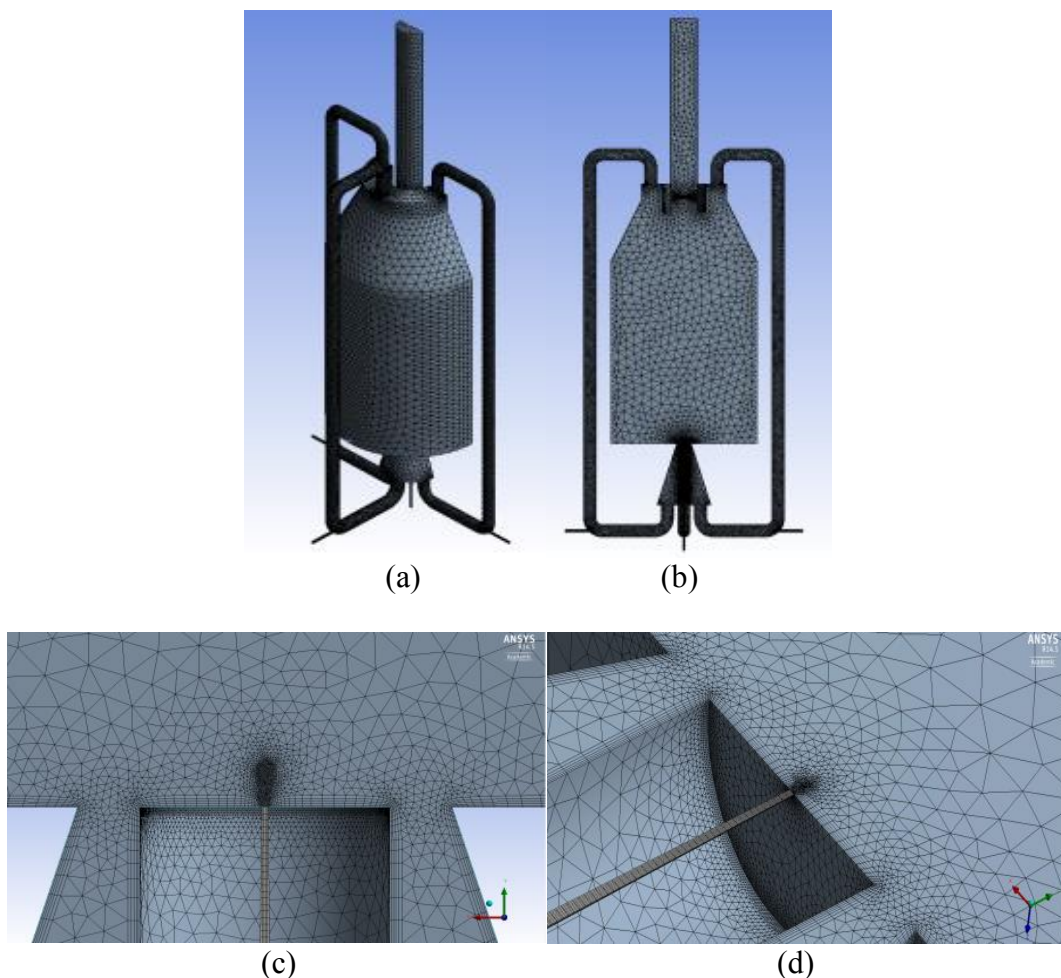


Figure 2. The model meshing with course mesh in the middle and fine mesh at critical locations, such as near walls or air and fuel nozzles (a) full meshing 3D view, (b) 2D view for meshing, (c) 2D view for fine mesh using body of influence at fuel and air nozzle inlet, (d) 3D view for fine mesh at fuel and air nozzle inlet

Meshing inflation is necessary at areas near the wall (Table 3). Stair stepping or layer compression is use to avoid collision. There are 5 layers with a growth rate of 20% and maximum thickness of 2.0mm. The nozzle inlet is very small and needs special meshing treatment, such as use of the sweep method, face sizing and edge sizing. A number of divisions is selected for the edge sizing technique. In the area where the fuel

jets mixes with the air jet, a super fine mesh is needed, and this can be provided by using the body sizing meshing technique. There are 3 types of body sizing: element size, sphere of influence and body of influence. For the body of influence, the scope geometry is the whole body selection and a frozen body needs to be added and drawn in the design model as in Figure 3(a). The mesh result for the body of influence, shown in Figure 3(b), is very sensitive and the process needs to be repeated until it is stable (repeat by removing the frozen body, drawing again). The sphere of influence will give a higher number of nodes and elements. The sphere center and radius need to be selected, normally using the xy-plane as in Figure 3(c). The mesh result is shown in Figure 3(d).

Table 2. Statistics on nodes, elements and mesh metrics for skewness and aspect ratio.

Item	Beginning setting	Final setting
Nodes	75,460	244,650
Elements	197,747	700,161
Mesh metric	Skewness	Skewness
Min	2.448399E-04	8.116788E-05
Max	0.981734	0.845774
Average	0.357655	0.227029
Standard deviation	0.164923	0.127163
Mesh metric	Aspect Ratio	Aspect Ratio
Min	1.165	1.053
Max	649.49	209.09
Average	15.940685	9.202309
Standard deviation	34.301834	15.52761

Table 3. The parameter settings for inflation.

Item	Setting
Use automatic inflation	Program controlled
Inflation option	Total thickness
Inflation algorithm	Pre
View advanced option	Yes
Collision avoidance	Stair stepping
Growth rate type	Geometric
Use post smoothing	Yes
Number of layers	5
Growth rate	1.2
Maximum thickness	2.mm
Gap factory	0.5
Maximum height over base	1
Maximum angle	140.0
Fillet ratio	1
Smoothing iterations	5

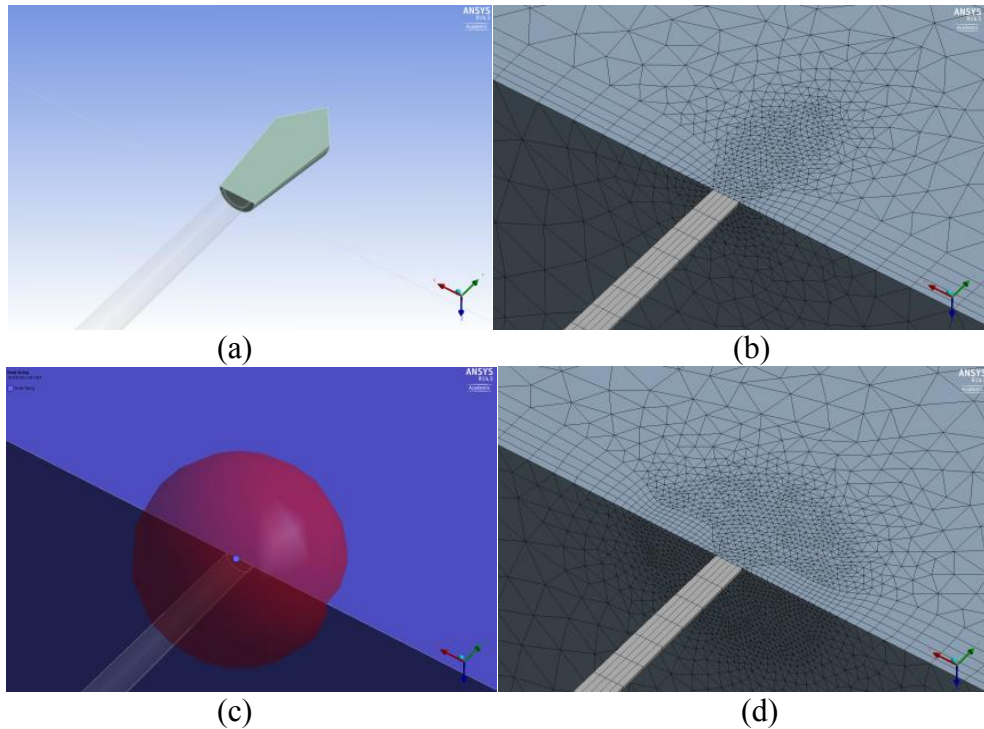


Figure 3. Body sizing mesh for (a) geometry of body of influence, (b) meshing of body of influence, (c) geometry of sphere of influence, (d) meshing of sphere of influence

In order to simulate and access the high accuracy of the modeling, and to ensure that mesh independence is applied, a grid independence study was performed for different mesh settings. Grids A, B, C and D were generated to simulate the temperature profile in the combustion chamber. The maximum skewness was 0.873, 0.898, 0.882 and 0.888 for grid A, B, C and D respectively, which is below the allowable limit of 0.98. Maximum skewness must be below 0.98 or the solution will easily become a divergence error and will not converge as desired. Temperature distribution was measured in the middle of the chamber and the result is as depicted in Figure 4. Figure 4(a) - (d) show the different grid sizes of grids A, B, C and D. The cross-section of the chamber marked as X-X axis is generated in the model in Figure 4 to compare the temperature reading in this axis. As a result, Grids C and D give almost identical results as shown in Figure 5.

The results show that the temperature profiles in Grids C and D are smoother and produce a better temperature distribution, including near the wall. The temperature variation can be seen in Figure 5, of 0.47%, 0.58%, 0.23% and 0.23% for Grids A, B, C and D respectively. This shows that Grids C and D give better and lower variance than Grids A and B. The difference between both temperature profiles is clearly seen in the region 5mm from the wall. Figure 5 shows the combustion chamber temperatures for Grids A, B, C and D. The majority of both domains are close to the average temperature of the combustion chamber: for Grids C and D the temperature range is 864K to 866K which shows that the temperature was identical and the grid was independent. According to the above results, Grid C demonstrates a better solution and result, and so was selected for the rest of the simulation study.

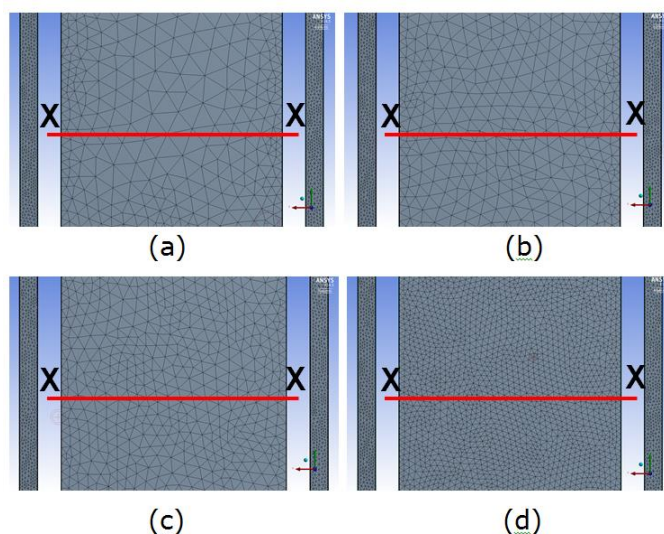


Figure 4. Meshing independence (a) mesh grid A,(b) mesh grid B,(c) mesh grid C,(d) mesh grid D.

MODELLING SOLUTION SETUP

Single or double precision must be set as an option during solution setup. If double precision is used, the solution will be slower, and this is not necessary for many cases. The processing option involves the setting of a single or parallel processor on a local machine. A maximum of four parallel computer processors can be used with one license. This is applicable to multicore processor computers, but not single processor computers. To increase the parallel processor to more than four, a second license is needed. The steps are as follows:

Ensure the unit for the model is correctly setup in general settings. Record the extended measurement for the domain since it may be required when the setting plane cutting, in order to view the result. Check the report quality to ensure the mesh quality is acceptable. An orthogonal quality range is from 0 to 1, where the lower value means lower quality. In this case the minimum orthogonal quality is 0.129378. The solver setting is dependent on the type of solver, and will be in between pressure-based and density based. Solver selection is also needed for the velocity formulation setting, which is between absolute and relative, and for the time between steady or transient solution. This case uses pressure-based, absolute velocity and a steady solver. The gravitational acceleration settings are in Y direction at -9.81m/s^2 . The most important setting is that for models since these parameter settings are related to the simulation conditions, including energy, radiation, turbulent viscosity and species. The energy equation must be turned on as there will be temperature change in the combustion process. The turbulent viscous model selection is the realizable k-epsilon with a standard wall function as near wall treatment. The discrete ordinate (DO) is chosen for the radiation and non-premixed is chosen for species. Some of the settings will be further explained in next section. The Probability Density Function (PDF) table creation boundary condition for the fuel and oxidant was set as shown in Table 4. The biogas fuel was created by mixing methane (60%) and carbon dioxide (40%) on a molar basis. This biogas mixing ratio was also used by other researchers (Colorado, Herrera, & Amell, 2010; Keramiotis & Founti, 2013; Salunkhe, Rai, & Borkar, 2012) in their biogas research. For the oxidant, the mixing of nitrogen (79%) and oxygen (21%) was used as

the normal combustion air configuration. The fuel and oxidant temperature was set at 300K.

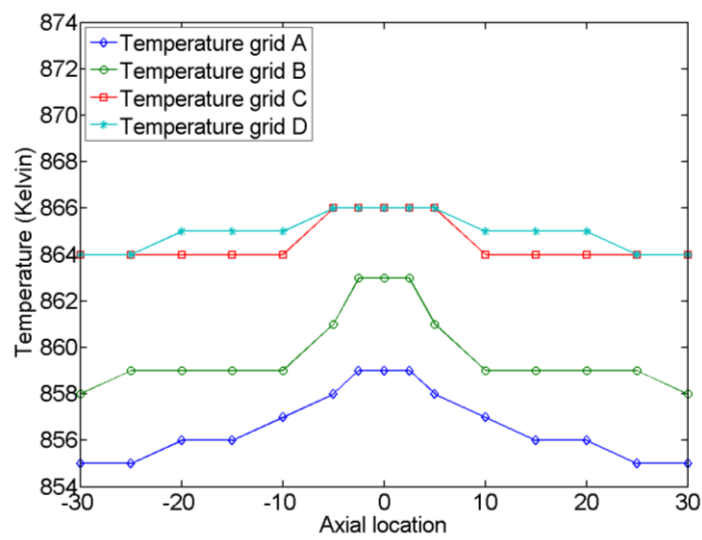


Figure 5. Temperature distribution for X-X axis for grid A, B, C and D.

Table 4. PDF table creation for boundary condition parameters.

Species	Fuel	Oxidant
CH ₄	0.60	0
N ₂	0	0.79
O ₂	0	0.21
CO ₂	0.40	0

PDF mixture is used for the material and the species count is dependent on the model setting (Table 5). The pressure is set at 101.325kPa and the fuel stream rich flammability limit is set as Table 5 for model setting under the setting for non-premixed combustion.

Table 5. PDF table creation for model setting parameters for fuel stream rich flammability limit (FSRFL).

Oxygen level (%)	Stoichiometric FSRFL	Stoichiometric FSRFL + 10%	Species
1	0.015	0.0165	8
3	0.024	0.0264	8
5	0.038	0.0418	8
7	0.052	0.0572	9
9	0.066	0.0726	11
11	0.080	0.088	11
13	0.092	0.1012	13
15	0.105	0.1155	13
17	0.117	0.1287	13
19	0.130	0.1430	14
21	0.142	0.1562	16
23	0.155	0.1705	17
25	0.167	0.1837	18
27	0.178	0.1958	18

After this setting is confirmed, set the inlet diffusion at the PDF option with automated grid refinement. The next step is to calculate PDF table and display the results. The PDF table can be checked by displaying the PDF table, choosing the figure type as 2D or 3D, and which parameters to display (the default is the 3D figure: mean temperature, mean mixture fraction and scaled variance). The boundary condition is the setting for the inlet, wall and outlet. In this case there are four air inlets, one fuel inlet, one exhaust and one wall for the whole chamber. For the air inlet and fuel inlet, the momentum setting for the velocity specification method uses the component method. The Cartesian coordinate system was used in line with the model coordinate system. The velocity for the air inlet was in the x and z direction. Under the thermal setting, the temperature was set to 300K and for the species setting; the mean mixture fraction was set to zero. The velocity for the fuel inlet was in Y direction and thermal (temperature) setting was 300K, but the mean mixture fraction was set to unity. The turbulence specification method was 'intensity', the hydraulic diameter which involves turbulence intensity was set to 5% and the hydraulic diameter to 10mm as per model measurement. The velocity for the air and fuel inlet, in unit m/s, is one of the main parameters to change, depending on the air fuel ratio of the biogas and oxidant (Noor, Wandel, et al., 2012). The wall setting is 'stationary wall' and 'no slip shear' condition with thermal heat flux 0 w/m^2 and an internal emissivity of one.

MODELLING SOLUTION

The solution of the simulation involves chemical reactions since it is a non-premixed combustion process, involving heat transfer, turbulent flows and species transport. The simulation used Reynolds-Averaged Navier–Stokes (Lindberg, Hörlin, & Göransson) equations solved together with a realizable k- ϵ turbulence model (Shih, Liou, Shabbir, Yang, & Zhu, 1995) [that was developed based on the standard k- ϵ turbulence model (Launder & Spalding, 1974)] solved using commercial CFD software ANSYS Fluent 14.5 (Fluent Inc, 2012). The discrete ordinate (DO) radiation model (Chui & Raithby, 1993; Fiveland, 1984) and absorption coefficient of the weighted sum of gray gas (WSGGM) model (Hottel & Sarofim, 1967; Smith, Shen, & Friedman, 1982; Soufiani & Djavdan, 1994) was used in this work. The selection of the WSGGM model is suitable for this work as it gives a reasonable compromise between oversimplified gray gas assumption and the complete model, accounting for the entire spectral variation of radiation properties (Yeoh & Yuen, 2009). The solution method setting (Table 6) shows the original and new settings for the case. The couple method is used for the pressure-velocity coupling scheme with least square cell based gradient and presto for pressure. The second order upwind is suitable for the momentum, turbulent kinetic energy, turbulent dissipation rate, pollutant no, energy, discrete ordinates, mean mixture fraction, and mixture fraction variance, when the solution is run in the final stage.

The solution control for flow Courant number, explicit relaxation factor (ERF) and under-relaxation factor (Alfriend, Vadali, Gurfil, How, & Breger) is shown in Table 7. At the beginning of the simulation, the calculations need to be run with the original values of the parameter settings and the result evaluated. In many complex cases where the simulation includes chemical reactions such as combustion, the original setting will give a divergence error and need more attention. If the solution is diverged, the flow Courant number and relaxation factor need to change depending on the error of divergence. In this case, the error is enthalpy and the new setting reduces the flow Courant number from 200 to 50 and reduces the relaxation factor for momentum,

pressure and density as shown in Table 7. The reduction of the relaxation factor will slow the convergence process.

Table 6. The parameter setting for the solution method.

Parameters	Original Setting	New Setting
Pressure-velocity coupling	Simple	Couple
Gradient	Green-gauss cell based	Least squares cell based
Pressure	standard	PRESTO!
Momentum	First order upwind	Second order upwind
Turbulent kinetic energy	First order upwind	Second order upwind
Turbulent dissipation rate	First order upwind	Second order upwind
Pollutant no	First order upwind	Second order upwind
Energy	First order upwind	Second order upwind
Discrete ordinates	First order upwind	Second order upwind
Mean mixture fraction	First order upwind	Second order upwind
Mixture fraction variance	First order upwind	Second order upwind

Table 7. Solution control parameters for flow Courant number, explicit relaxation factor and under-relaxation factor.

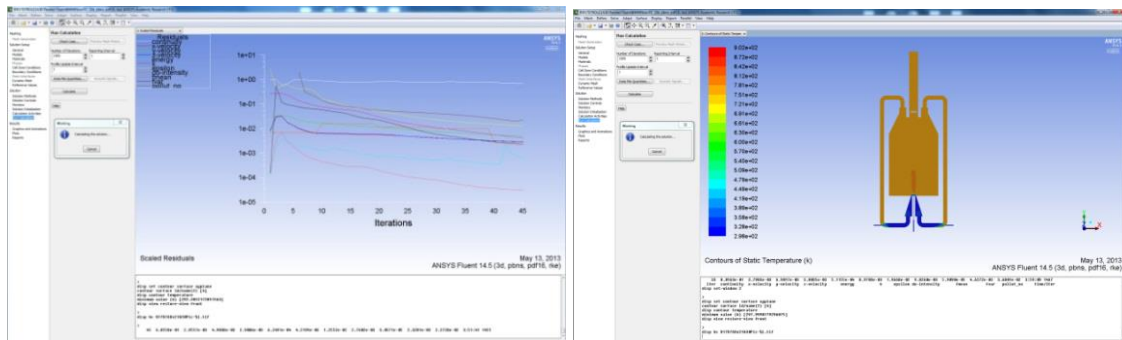
Parameters	Original Value	New Value
Flow courant number	200	50
ERF: momentum	0.75	0.3
ERF: pressure	0.75	0.45
URF: density	1.0	0.3
URF: body force	1.0	1.0
URF: turbulent kinetic energy	0.8	0.8
URF: turbulent dissipation rate	0.8	0.8
URF: turbulent viscosity	1.0	1.0
URF: pollutant no	0.9	0.9
URF: energy	1.0	1.0
URF: temperature	1.0	1.0
URF: discrete ordinates	1.0	1.0
URF: mean mixture fraction	1.0	1.0
URF: mixture fraction variance	0.9	0.9

The residual of convergence criteria use is absolute for monitoring the calculation process, and the criteria is set at $1e-16$ to ensure the convergence process is smooth. The initial processes use the hybrid and the setting is automatically pre-set by the software, then the patch is dependent on the model's need. In this case the patch is used for Y velocity, then needed to force the flow downward (negative Y) for the exhaust gas recirculation (Chen, Wegrzyn, & Prasad) to the pipe. The patch for Y velocity is -10m/s. The second patch is for temperature: 350K. This is about 50K above room temperature. For calculation activities, we use execute commands (Table 8) to generate a series of images, step by step, and combine the images using the image sequence in Apple QuickTime or other software: those images will become a movie of the flame from start to end of the iterations. The file name in this case is B17AN14D76FN10x21A15Pic-%i.tif and a *.tif file will be save for every

individually iteration. The iteration pictures that are generated by that command will be saved as running numbers with 0001 to 9999 at the end of the filename (B17AN14D76FN10x21A15Pic-0001.tif). The display during the calculation will be shown as Figure 6, where residual monitoring is in Window 1 (Figure 6(a)) and the xy-plane contour surface in Window 2 (Figure 6(b)).

Table 8. Execute commands under calculation activities.

Numbering	Iterations	Command
Command-1	1 Iteration	disp set-window 2
Command-2	1 Iteration	disp set contour surface xy-plane
Command-3	1 Iteration	disp contour temperature
Command-4	1 Iteration	disp view restore-view front
Command-5	1 Iteration	disphc B17AN14D76FN10x21A15Pic-%i.tif



(a)

(b)

Figure 6. Monitoring window during calculation (a) Window 1, (b) Window 2

Before the calculation process starts, a case check needs to be made to ensure that there are no errors and that the model is ready to be simulated. The check case checks the mesh, models, boundaries and cell zone, materials and solver. In this example, the calculation was set up at 4500 iterations, as in Figure 7. The calculation was converging and the result was satisfied when non-premixed combustion occurred and MILD achieved as expected. There was much trial and error to achieve the convergence, especially of the explicit relaxation factor (ERF) and under-relaxation factor (Alfriend et al.). Figure 8 shows one of the examples of common error which is a primitive error at Node 1: a floating point exception (divergence detected in AMG solver: enthalpy or some time the error of divergence detected in AMG solver: epsilon). To solve this error flow, the Courant number and three relaxation factor is tested and finally reaches the optimum values.

The convergence of the solution is very important to ensure that the end result of the simulation is correct and accurate. The relaxation method may be used to accelerate or delay the solution, using the relaxation factor. The relaxation factor (λ) can be seen in the equation below,

$$\phi_{i,j,k}^{new} = \lambda \phi_{i,j,k}^p + (1 - \lambda) \phi_{i,j,k}^{p-1} \tag{8}$$

where λ is between 1-2 and $\phi_{i,j,k}^p$ is the value from the present iteration and $\phi_{i,j,k}^{p-1}$ is the value from the past iteration. The convergence can be monitored by the residual (Figure 7 and 8). If λ is less than 1.0, this is under-relaxation and will slow down the convergence and the simulation will take longer. Under-relaxation will increase the calculation stability and reduce the divergence possibility. If λ is equal to 1.0, it means there is no relaxation applied. If λ is more than 1.0, it is over-relaxation.

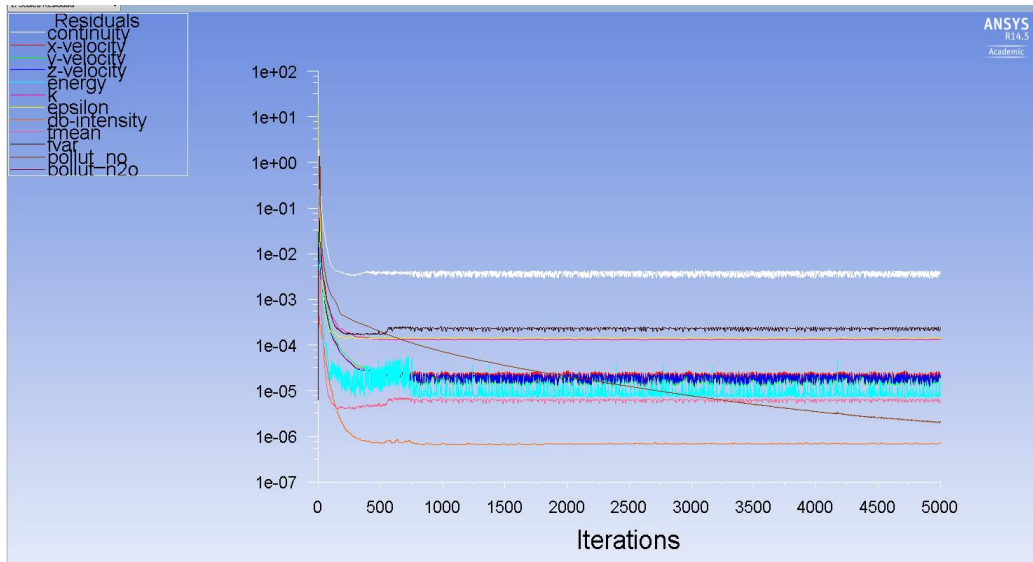


Figure 7. Converge solution

Over-relaxation will accelerate the convergence but at the same time will reduce the calculation stability and give a high probability of the solution diverging. The most sensitive relaxation factors in the combustion simulation are energy, temperature, radiation (discrete ordinates) and mean mixture fraction. These items will normally use 1.0 as relaxation factors. For an under-relaxation factor (Table 7), it is advice is to use a high relaxation factor (near to or 1.0) since if it too low, the convergence will be too slow and may not be converged, even if it appears to converge. The default relaxation factor is the factor proposed by the solver and if the solution is still diverged, the explicit relaxation factor (momentum and pressure) can be reduced to slow convergence (Table 7).

MODELLING RESULTS

The result of the simulation can be presented in a graphical view or in numerals as flow fields through the export function (File → Export → Solution data). The options for the graphical result are contours plots, vector plots, iso-surface plots or animations. The most commonly used are contour plots and vector plots. The results shown in Figure 9 are from contours in the graphics. The option was set as filled, node values, and global range, and the contour on Figure 9(a) is a 2D view of the velocity magnitude from the xy-plane. The plane was set at the surface option and then selected. The plane surface setting used to create the xy-plane is shown in Table 9. The temperature contour result (Figure 9(b)) was in two planes on the 2D view, xy-plane and yz-plane, created by the same technique as the xy-plane. The temperature contour is homogeneous throughout the combustion chamber, showing that MILD combustion was achieved. The

convergence of the simulation is considered achieved if the residual is stable or there is no more change from one iteration to the next iteration (Figure 7). If the residual has already achieved the lower limit set by the residual monitor but is still showing a reducing trend, the solution may not be converged until the residual is stable. The lower limit for the residual is normally set at 1.0×10^{-6} . In some cases the lower limit is set at between 1.0×10^{-3} to 1.0×10^{-6} .

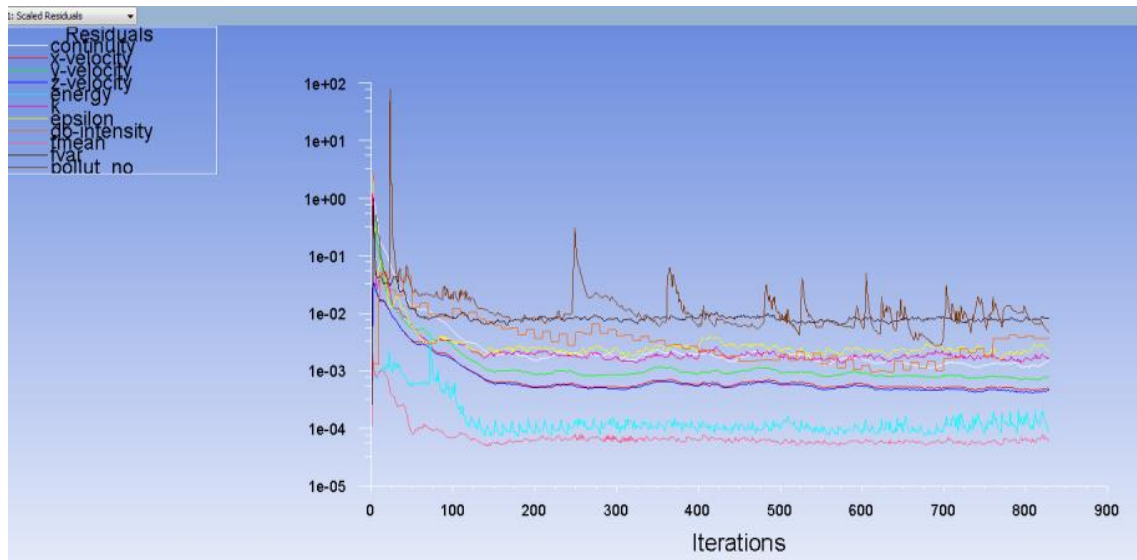


Figure 8. Error on divergence detected in AMG solver: enthalpy

Table 9. Point for 2D xy-plane setting the view contour result

x0	x1	x2
-486mm	-486mm	486mm
y0	y1	y2
-438mm	-438mm	1750
z0	z1	z2
0	0	0

The results or post-processing from the ANSYS workbench component system (ANSYS Results) show the flow streamline (Figure 10) and the wall contour (Figure 10(c)) and can be developed and analyzed. Figure 10(a) shows the 3D velocity streamline for all domains with 25 point sampling equally spaced from the fuel inlet in a forward and backward direction. Figure 10(b) shows the same setting but starts from air inlet 1. The streamlining is more than the fuel inlet since the volume of the air inlet is higher than that of the fuel inlet. For both streamlines, the downward flow through the EGR pipe can be seen clearly. Some exhaust flow from the exhaust outlet can be seen in Figure 10(b). The contour result for the wall temperature can be plotted. The wall temperature is in the range of 983 to 1012 K and is homogenously distributed. The temperature for the EGR pipe wall is reduced from 983 to 1012K at the top (early of EGR) and reduces to a range of 537 to 636K before mixing with fresh air at 300K. When the hot flue gas (Chen et al.) mixed with fresh air, the mixing temperature decreased further to the range of 418 to 537K before re-entering the combustion chamber. This condition can be seen as fresh air preheated by the EGR from 300K to the range of 418 to 537K. The oxygen content in the fresh air was also diluted and this

preheating and dilution of the oxidant causes the furnace to achieve a MILD combustion regime.

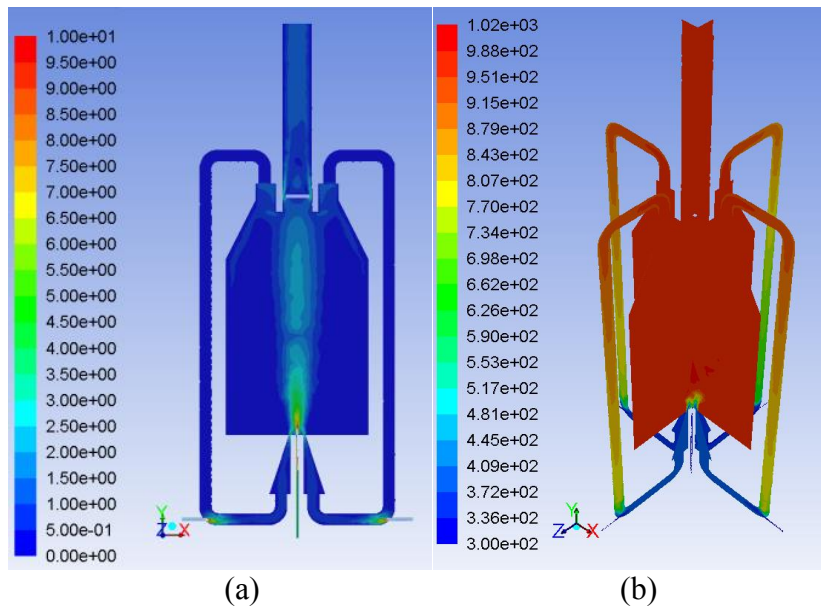


Figure 9. The contour result for (a) 2D view for velocity magnitude (unit: m/s), (b) 3D view for temperature distribution (units: Kelvin).

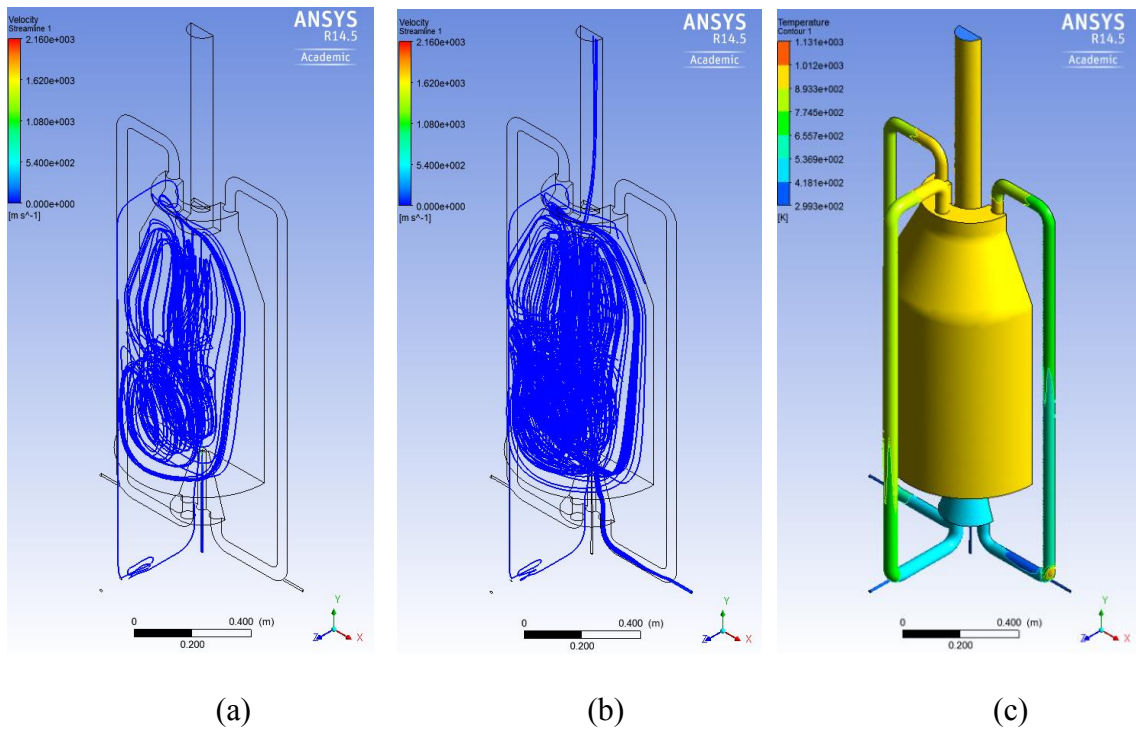


Figure 10. The velocity streamlines (a) start from fuel inlet, (b) start from air inlet, (c) temperature contour on the furnace wall.

CONCLUSIONS

The CFD simulation was completed and in summary, below conclusions can be drawn from the simulation of non-premixed MILD combustion.

- i. The most important and critical step in CFD work is meshing. The quality of meshing has the highest influence on whether the calculations will converge and produce good results or diverge and give an erroneous result.
- ii. The meshing quality can be checked by the skewness, aspect ratio on mesh metrics and smoothness. The maximum skewness must not exceed 0.98.
- iii. The selection of the solution method and solution control must be suitable for the model and equation to be solved.
- iv. Divergence of the solution can commonly be solved by changing the explicit under relaxation factors. The advisable changing rate is about 10% for each new simulation.
- v. Residual monitoring is a very useful tool to monitor the iteration steps and whether they converge or diverge. The residual will be converged when the value is stable and not decreasing.
- vi. The fresh air was preheated by the EGR from 300K to the range of 418 to 537K and the oxygen was diluted, resulting in the burner achieving MILD combustion conditions as expected.
- vii. The simulation successfully achieved the objectives of the MILD regime where the ratio of maximum-to-average temperature was less than the required 23% for MILD conditions.

ACKNOWLEDGMENTS

The authors would like to thank the University of Southern Queensland (USQ), Ministry of Higher Education, Malaysia (MOHE) and Universiti Malaysia Pahang (Bumpus) for providing financial support and laboratory facilities.

REFERENCES

- Acon, C., Sala, J., & Blanco, J. (2007). Investigation on the design and optimization of a low nox-co emission burner both experimentally and through cfd simulations. *Energy and Fuels*, 21(1), 42-58.
- Alfriend, K., Vadali, S. R., Gurfil, P., How, J., & Breger, L. (2010). *Spacecraft formation flying: Dynamics, control, and navigation* (Vol. 2): Butterworth-Heinemann.
- Arghode, V. K., & Gupta, A. K. (2011). Development of high intensity cdc combustor for gas turbine engines. *Applied Energy*, 88(3), 963-973.
- Baukal Jr, C. E., Gershtein, V., & Li, X. J. (2000). *Computational fluid dynamics in industrial combustion*. New York: CRC press.
- Bumpus, S. R. J. (2002). *Experimental setup and testing of fiber reinforced composite structures*. (Master), University of Victoria.
- Cavaliere, A., & Joannon, D. M. (2004). Mild combustion. *Progress in Energy and Combustion Science*, 30, 329-366.

- Chen, L., Yong, S. Z., & Ghoniem, A. F. (2012). Oxy-fuel combustion of pulverized coal: Characterization, fundamentals, stabilization and cfd modeling. *Progress in Energy and Combustion Science*, 38(2), 156-214.
- Chen, Q.-S., Wegrzyn, J., & Prasad, V. (2004). Analysis of temperature and pressure changes in liquefied natural gas (Lng) cryogenic tanks. *Cryogenics*, 44(10), 701-709.
- Chui, E., & Raithby, G. (1993). Computation of radiant heat transfer on a nonorthogonal mesh using the finite-volume method. *Numerical Heat Transfer*, 23(3), 269-288.
- Colorado, A., Herrera, B., & Amell, A. (2010). Performance of a flameless combustion furnace using biogas and natural gas. *Bioresource Technology*, 101(7), 2443-2449.
- Dally, B. B., Shim, S. H., Craig, R. A., Ashman, P. J., & Szegö, G. G. (2010). On the burning of sawdust in a mild combustion furnace. *Energy & Fuels*, 24(6), 3462-3470.
- Davidson, D. L. (2002). The role of computational fluid dynamics in process industries. *The Bridge*, 32(4), 9-14.
- Devi, R., Saxena, P., Walter, B., Record, B., & Rajendran, V. (2004). Pressure reduction in intake system of a turbocharged-inter cooled di diesel engine using cfd methodology: SAE Technical Paper.
- Duwig, C., Stankovic, D., Fuchs, L., Li, G., & Gutmark, E. (2007). Experimental and numerical study of flameless combustion in a model gas turbine combustor. *Combustion Science and Technology*, 180(2), 279-295.
- Fiveland, W. (1984). Discrete-ordinates solutions of the radiative transport equation for rectangular enclosures. *Journal of Heat Transfer*, 106(4), 699-706.
- Fletcher, D., Haynes, B., Christo, F., & Joseph, S. (2000). A cfd based combustion model of an entrained flow biomass gasifier. *Applied Mathematical Modelling*, 24(3), 165-182.
- Fluent Inc. (2012). Fluent 14.5 user's guide.
- Hairuddin, A. A., Yusaf, T. F., & Wandel, A. P. (2011). *Predicting the combustion behaviour of a diesel hcci engine using a zero-dimensional single-zone model*. Paper presented at the Proceedings of the Australian Combustion Symposium 2011, Newcastle, Australia.
- Hasegawa, T., Mochida, S., & Gupta, A. (2002). Development of advanced industrial furnace using highly preheated combustion air. *Journal of propulsion and power*, 18(2), 233-239.
- Hottel, H. C., & Sarofim, A. F. (1967). *Radiative transfer*. New York: McGraw Hill.
- IEA. (2009). World energy outlook. Paris: International Energy Agency.
- Jones, W., & Launder, B. (1972). The prediction of laminarization with a two-equation model of turbulence. *International Journal of Heat and Mass Transfer*, 15(2), 301-314.
- Katsuki, M., & Hasegawa, T. (1998). The science and technology of combustion in highly preheated air. *Symposium (International) on combustion*, 27(2), 3135-3146.
- Keramiotis, C., & Founti, M. A. (2013). An experimental investigation of stability and operation of a biogas fueled porous burner. *Fuel*, 103, 278-284.
- Khelil, A., Naji, H., & Loukarfi, L. (2007). Numerical study of swirling confined non-premixed flames with determination of pollutant emissions. *International Review of Mechanical Engineering*, 1(6), 618-627.

- Launder, B., & Sharma, B. (1974). Application of the energy-dissipation model of turbulence to the calculation of flow near a spinning disc. *Letters in heat and mass transfer*, 1(2), 131-137.
- Launder, B. E., & Spalding, D. (1974). The numerical computation of turbulent flows. *Computer Methods in Applied Mechanics and Engineering*, 3(2), 269-289.
- Li, P., Mi, J., Dally, B. B., Wang, F., Wang, L., Liu, Z. et al. Zheng, C. (2011). Progress and recent trend in mild combustion. *Science China Technological Sciences*, 54(2), 255-269.
- Lindberg, E., Hörlin, N.-E., & Göransson, P. (2013). An experimental study of interior vehicle roughness noise from disc brake systems. *Applied Acoustics*, 74(3), 396-406.
- Maczulak, A. (2010). *Renewable energy: Sources and methods*. New York: Facts on File Inc.
- Majda, A., & Sethian, J. (1985). The derivation and numerical solution of the equations for zero mach number combustion. *Combustion Science and Technology*, 42(3-4), 185-205.
- Najiha, M. A., Rahman, M. M., Kamal, M., Yusoff, A. R., & Kadirgama, K. (2012). Mql flow analysis in end milling processes: A computational fluid dynamics approach. *Journal of Mechanical Engineering and Sciences*, 3, 340-345.
- Noor, M., Hairuddin, A. A., Wandel, A. P., & Yusaf, T. (2012). Modelling of non-premixed turbulent combustion of hydrogen using conditional moment closure method. *IOP Conference Series: Materials Science and Engineering*, 36, 1-17.
- Noor, M., Wandel, A. P., & Yusaf, T. (2012). A review of mild combustion and open furnace design consideration. *International Journal of Automotive and Mechanical Engineering*, 6(1), 730-754.
- Noor, M., Wandel, A. P., & Yusaf, T. (2013). *The analysis of recirculation zone and ignition position of non-premixed bluff-body for biogas mild combustion*. Paper presented at the Proceedings of the 2nd International Conference of Mechanical Engineering Research, Malaysia.
- Noor, M. M., Wandel, A. P., & Yusaf, T. (2013a). Analysis of recirculation zone and ignition position of non-premixed bluff-body for biogas mild combustion. *International Journal of Automotive and Mechanical Engineering*, 8, 1176-1186.
- Noor, M. M., Wandel, A. P., & Yusaf, T. (2013b). Design and development of mild combustion burner. *Journal of Mechanical Engineering and Sciences*, 5, 662-676.
- Peters, N. (2004). *Turbulent combustion*. UK: Cambridge University Press.
- Press, W. H., Teukolsky, S. A., Vetterling, W. T., & Flannery, B. P. (1992). *Numerical recipes in fortran*. UK: Cambridge University Press.
- Rahimi, M., Khoshhal, A., & Shariati, S. M. (2006). Cfd modelling of a boilerstubes rupture. *Applied Thermal Engineering*, 26, 2192-2200.
- Ramasamy, D., Noor, M. M., Kadirgama, K., Mahendran, S., Redzuan, A., Sharifian, S. A., & Buttsworth, D. R. (2009). *Validation of drag estimation on a vehicle body using cfd*. Paper presented at the Europe Power and Energy Systems, Spain.
- Rehm, R., & Baum, H. (1978). The equation of motion for thermally driven bouyant flows. *N. B. S. J. Res*, 83, 297-308.
- Salunkhe, D., Rai, R., & Borkar, R. (2012). Biogas technology. *International Journal of Engineering Science and Technology*, 4(12), 4934-4940.

- Shafiee, S., & Topal, E. (2009). When will fossil fuel reserves be diminished? *Energy Policy*, 37(1), 181-189.
- Shih, T.-H., Liou, W. W., Shabbir, A., Yang, Z., & Zhu, J. (1995). A new k- ϵ eddy viscosity model for high reynolds number turbulent flows. *Computers & Fluids*, 24(3), 227-238.
- Smith, T., Shen, Z., & Friedman, J. (1982). Evaluation of coefficients for the weighted sum of gray gases model. *Journal of Heat Transfer*, 104(4), 602-608.
- Soufiani, A., & Djavdan, E. (1994). A comparison between weighted sum of gray gases and statistical narrow-band radiation models for combustion applications. *Combustion and Flame*, 97(2), 240-250.
- Tsuji, H., Gupta, A., Hasegawa, T., Katsuki, M., Kishimoto, K., & Morita, M. (2003). *High temperature air combustion, from energy conservation to pollution reduction*. Boca Raton, FL: CRC Press.
- Verissimo, A., Rocha, A., & Costa, M. (2013). Importance of the inlet air velocity on the establishment of flameless combustion in a laboratory combustor. *Experimental Thermal and Fluid Science*, 44, 75-81.
- Wandel, A. P. (2011). *A stochastic micro mixing model based on the turbulent diffusion length scale*. Paper presented at the Australia Combustion Symposium, Newcastle, Australia.
- Wandel, A. P. (2012). *Extinction precursors in turbulent sprays*. Paper presented at the International Symposium on Combustion, Poland.
- Wandel, A. P., Smith, N. S., & Klimenko, A. (2003). Implementation of multiple mapping conditioning for single conserved scalar *Computational fluid dynamics 2002* (pp. 789-790): Springer.
- Wünning, J. (1991). Flammenlose oxidation von brennstoffmithochvorgewärmterluft. *ChemieIngenieurTechnik*, 63(12), 1243-1245.
- Yeoh, G. H., & Yuen, K. K. (2009). *Computational fluid dynamics in fire engineering: Theory, modelling and practice*: Butterworth-Heinemann.
- Yusaf, T., Noor, M., & Wandel, A. P. (2013). *Mild combustion: The future for lean and clean combustion*. Paper presented at the Proceedings of the 2nd International Conference of Mechanical Engineering Research (ICMER 2013), Malaysia.